Doping-induced bandgap narrowing in Si rich n- and p-type Si_{1-x} Ge_x

2003 J. Phys.: Condens. Matter 15 489

(http://iopscience.iop.org/0953-8984/15/3/313)

INSTITUTE OF PHYSICS PUBLISHING JOURNAL OF PHYSICS: CONDENSED MATTER

J. Phys.: Condens. Matter **15** (2003) 489–502 PII: S0953-8984(03)35780-7

Doping-induced bandgap narrowing in Si rich n- and p-type $Si_{1-x}Ge_x$

S van Teeffelen[1], C Persson[1,2,3], O Eriksson[1] and B Johansson[1,2]

[1] Condensed Matter Theory Group, Department of Physics, Uppsala University, Box 530, SE-751 21 Uppsala, Sweden
[2] Department of Materials Science and Engineering, Royal Institute of Technology, SE-100 44 Stockholm, Sweden

E-mail: Sven.vanTeeffelen@fysik.uu.se

Received 11 April 2002, in final form 25 September 2002
Published 13 January 2003
Online at stacks.iop.org/JPhysCM/15/489

Abstract

The shifts of the fundamental and optical bandgap energies as functions of dopant concentration in heavily n-type and p-type doped $Si_{1-x}Ge_x$ ($x \leqslant 0.3$) have been investigated theoretically. The band structure of the intrinsic crystal was described by the $\boldsymbol{k} \cdot \boldsymbol{p}$-perturbation method, where the Kohn–Luttinger parameters were determined from a first-principles and full-potential band-structure calculation. The doping-induced effects on the bandgap were thereafter calculated using a zero-temperature Green function formalism within the random phase approximation and with a local field correction of Hubbard. We found only small effects on the bandgap energies due to variation of composition x. The calculated bandgap narrowing of Si and of $Si_{0.82}Ge_{0.18}$ were found to be in good agreement with photoluminescence measurements.

1. Introduction

Doping has a strong influence on the electronic properties of a semiconductor, especially on the fundamental and optical bandgaps. This effect is important for the design of semiconductor devices. Heavily doped $Si_{1-x}Ge_x$ is for instance used in transistors in order to shrink the width of pn-junctions and in solar cells in order to improve the emitter efficiency. For further applications, see e.g. [1–3].

In this work, the effect of high concentration n-type and p-type doping (i.e., for concentrations above the Mott critical density [8]) of $Si_{1-x}Ge_x$ is studied. For these concentrations the donors (in n-type materials) can be regarded as fully ionized even at zero temperature, and the donor electrons thus form an electron gas in the conduction band [8]. Interactions occurring due to the presence of these electrons and the ionized donors change

[3] Current address: National Renewable Energy Laboratory, 1617 Cole Boulevard Golden, CO 80401, USA.

the physical properties of the crystal, for instance the total energy. The different interactions contributing to the change of the total energy of the crystal are those

(i) between the electron gas and the ionized impurities,
(ii) between the electrons within the electron gas,
(iii) between the valence band electrons and the ionized impurities and
(iv) between the valence band electrons and the electron gas.

The additional energy is assumed to be a perturbation to the energy of the intrinsic crystal: $\hat{H} = \hat{H}^0 + \hat{H}^1$, where $\hat{H}^0$ is the unperturbed Hamiltonian and $\hat{H}^1$ is the perturbation Hamiltonian. The difference between the actual energy of a single electron in the doped crystal $E_j(\boldsymbol{k})$ and the energy of the corresponding electron in the undoped crystal $E_j^0(\boldsymbol{k})$ is the real part of the self-energy of the electron state: $E_j(\boldsymbol{k}) - E_j^0(\boldsymbol{k}) = \mathrm{Re}\,[\hbar\Sigma_j(\boldsymbol{k}, E_j^0(\boldsymbol{k})/\hbar)]$. n-type doping does not only have an effect on the electron states in the conduction bands but also on the electron states in the valence bands due to the screening of the electron gas. Usually, the self-energies of conduction band states are negative and the self-energies of valence band states are positive. The sum of the self-energy at the maximum of the uppermost valence band and the self-energy at the minimum of the lowest conduction band is the so called bandgap narrowing (BGN) of the fundamental bandgap. The description above is for n-type doped materials, but the corresponding holds for p-type doping. If the differences between n- and p-type doping are not explicitly mentioned further on in the text, both n- and p-type doping can be regarded to produce the same effect on the bandgap.

The valence band structure of the intrinsic crystal was described within the six-band $\boldsymbol{k}\cdot\boldsymbol{p}$-perturbation theory [4–7]. The numerical parameters for this perturbation theory are determined from a first-principle, full-potential linearized augmented plane wave (FPLAPW) calculation [9]. Thus, the non-parabolicity of the valence bands has been taken into account. The BGN was thereafter calculated with a zero-temperature Green function formalism within the random phase approximation (RPA) [10, 11] and with a local field correction of Hubbard [12].

Calculations of doping induced BGN in semiconductors were performed earlier. Jain and Roulston [13] used a semi-empirical method to obtain the BGN, and they also used spherical valence bands and approximated overlap integrals. Sernelius [14] and Persson *et al* [15, 16] calculated the BGN for other materials than $Si_{1-x}Ge_x$, for instance, GaAs and SiC. Sernelius [14] improved the BGN calculation by applying a more complete Green function method. Persson *et al* [15, 16] used the same Green function formalism as in [14], but they improved the description of the valence bands by incorporating a full band structure calculation. In the present calculation we follow the computational scheme of Persson *et al* [15, 16], however, now by using the $\boldsymbol{k}\cdot\boldsymbol{p}$-perturbation method to describe the valence bands. The difference is that instead of describing the bands with energy values for discrete $\boldsymbol{k}$-points, only three parameters are necessary in order to calculate the energies and overlap integrals of the three uppermost valence bands. The use of this method has the advantage of being a much faster calculation. The overlap integrals between the different valence bands are improved and, moreover, the Fermi surface can be well described also for p-type materials. Since the numerical parameters in the $\boldsymbol{k}\cdot\boldsymbol{p}$-method are determined from the results of the FPLAPW calculation, the valence bands are described accurately in a region near the Γ-point.

In this article, CGS units are used. In the performed calculations the lowest conduction band $c1$ and the three uppermost valence bands $v1$, $v2$, $v3$ have been considered. The $v1$-band is the uppermost valence band. Since we are only treating cubic materials, these valence bands are the so called heavy-hole, light-hole and spin–orbit bands.

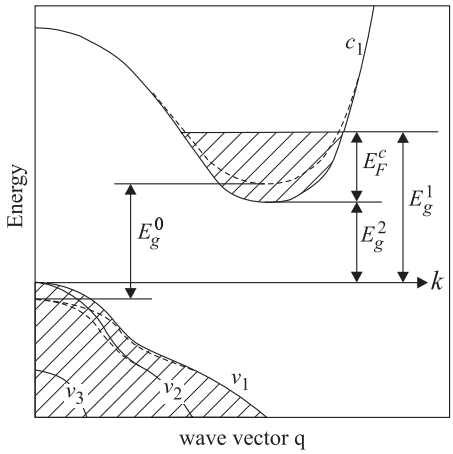

Figure 1. Schematic drawing of the energy bands of the intrinsic crystal (dashed curves) and of the shifted energy bands in a heavily doped n-type semiconductor (solid curves). The shaded parts show the occupied states up to the Fermi energy of the electron gas E_F^c. The optical bandgap E_g^1 and the reduced band gap E_g^2 are indicated as well as the fundamental bandgap of the intrinsic crystal E_g^0.

The effect of n-type doping above the Mott critical density is sketched in figure 1. The energy bands and the fundamental bandgap E_g^0 of the intrinsic crystal are indicated, as well as the energy bands, the optical E_g^1 and the reduced E_g^2 bandgaps of the doped crystal.

2. Computational method

2.1. Band structure of the intrinsic crystal

The calculation of the electronic structure of intrinsic $Si_{1-x}Ge_x$ (i.e., $E_j^0(\boldsymbol{k})$) was based on a first-principles, FPLAPW method [9]. The relativistic Hamiltonian was formulated within the local density approximation (LDA) to the density functional theory (DFT). We have chosen the exchange–correlation potential of Perdew and Wang [17], which is a parametrization of Ceperley–Alder data [18]. The band structure was calculated by using the experimental value [19] of the lattice constant: $a = 5.4310 + 0.2265x$ Å. The employed band-structure calculation has been found to describe the energy dispersion (i.e., the effective electron and hole masses) of intrinsic Si very accurately [20].

The LDA/DFT is well known to underestimate the fundamental band gap in semiconductors strongly. However, Si rich SiGe alloys have relatively large bandgap and scattering across the bandgap can therefore be neglected in the present Green function formalism. This means that the doping-induced energy shift of the bandgap ΔE_g does not depend on the value of the fundamental bandgap. Calculating the electronic structure of $Si_{1-x}Ge_x$ alloys we have applied an approach within the virtual-crystal approximation [21]. Since Si and SiGe have very similar bonds, the energy states of the $Si_{1-x}Ge_x$ valence electrons can be obtained approximatively as a linear combination of the corresponding Hamiltonians of the Si and SiGe valence states:

$$\hat{H}^{0,valence}_{Si_{1-x}Ge_x} = \hat{H}^{0,valence}_{Si}(1-2x) + \hat{H}^{0,valence}_{SiGe}2x$$
$$\hat{H}^{0}_{Si} = \hat{H}^{0,core}_{Si} + \hat{H}^{0,valence}_{Si_{1-x}Ge_x}$$
$$\hat{H}^{0}_{SiGe} = \hat{H}^{0,core}_{SiGe} + \hat{H}^{0,valence}_{Si_{1-x}Ge_x}.$$

The Kohn–Sham equations of $\hat{H}^0_{\mathrm{Si}}$ and $\hat{H}^0_{\mathrm{SiGe}}$ are both solved self-consistently with the FPLAPW method to obtain $\hat{H}^{0,valence}_{\mathrm{Si}_{1-x}\mathrm{Ge}_x}$. By using the valence Hamiltonian of SiGe ($\hat{H}^{0,valence}_{\mathrm{SiGe}}$) instead of the corresponding Hamiltonian of Ge, the total Hamiltonian of the valence states has zinc-blende ($\mathrm{T}^4_{\mathrm{d}}$) symmetry for $x > 0$ (and diamond, $\mathrm{O}^7_{\mathrm{h}}$, symmetry for $x = 0$). This is a more realistic treatment than using a Hamiltonian with $\mathrm{O}^7_{\mathrm{h}}$ symmetry also for $x > 0$, which was used by Krishnamurthy *et al* [22] in empirical pseudopotential calculations of the electronic structure of SiGe alloys. For instance, in contrast to the situation in the diamond structure, the two lowest conduction bands in the zinc-blende structure are non-degenerate at the X-point. This symmetry related splitting is important for the longitudinal effective electron mass $m^{\parallel}_{c1}$ since the mass value increases when the lowest conduction band becomes flatter due to the splitting. The transverse effective electron mass $m^{\perp}_{c1}$ is less affected. From the FPLAPW calculations, we found that the effective mass components for $x \leqslant 0.3$ can be written as

$$\begin{aligned} m^{\parallel}_{c1}(x) &= (0.971 + 0.159x)\, m_0 \\ m^{\perp}_{c1}(x) &= 0.193\, m_0, \end{aligned} \tag{1}$$

which for $x = 0$ are in good agreement with the experimental mass components of Si: $m^{\parallel}_{c1} = 0.92\, m_0$ and $m^{\perp}_{c1} = 0.19\, m_0$ [23]. The calculated energy dispersion of the lowest conduction band was found to be parabolic in the energy regime which is of importance in the present investigations. We therefore use a parabolic conduction band, represented by the effective masses of equation (1).

In order to speed up the BGN calculation the valence band structure of the intrinsic $\mathrm{Si}_{1-x}\mathrm{Ge}_x$ crystal is obtained using the $\boldsymbol{k}\cdot\boldsymbol{p}$-perturbation method [4–7], which is a method to obtain the energy values and eigenfunctions at $\boldsymbol{k}$-points that are near a $\boldsymbol{k}$-point (here, denoted $\boldsymbol{k}_0$) with well known energies and energy functions. The different energy states of the valence bands are the eigenvalues of the Kohn–Luttinger Hamiltonian [4, 5], a 6×6 matrix which for cubic materials and for $\boldsymbol{k}_0 = \boldsymbol{0}$ is given by

$$H = -\begin{pmatrix} H_{v1} & b & c & 0 & \mathrm{i}b/\sqrt{2} & -\mathrm{i}\sqrt{2}c \\ b^* & H_{v2} & 0 & c & -\mathrm{i}q & \mathrm{i}\sqrt{3/2}b \\ c^* & 0 & H_{v2} & -b & -\mathrm{i}\sqrt{3/2}b^* & -\mathrm{i}q \\ 0 & c^* & -b^* & H_{v1} & -\mathrm{i}\sqrt{2}c^* & -\mathrm{i}b^*/\sqrt{2} \\ -\mathrm{i}b^*/\sqrt{2} & \mathrm{i}q & \mathrm{i}\sqrt{3/2}b & \mathrm{i}\sqrt{2}c & H_{v3} & 0 \\ \mathrm{i}\sqrt{2}c^* & -\mathrm{i}\sqrt{3/2}b^* & \mathrm{i}q & \mathrm{i}b/\sqrt{2} & 0 & H_{v3} \end{pmatrix}. \tag{2}$$

The elements in the matrix are

$$H_{v1} = \frac{\hbar^2}{2m_0}[(\gamma_1 + \gamma_2)(k_x^2 + k_y^2) + (\gamma_1 - 2\gamma_2)k_z^2] \tag{3a}$$

$$H_{v2} = \frac{\hbar^2}{2m_0}[(\gamma_1 - \gamma_2)(k_x^2 + k_y^2) + (\gamma_1 + 2\gamma_2)k_z^2] \tag{3b}$$

$$H_{v3} = (H_{v1} + H_{v2})/2 + \Delta_0 \tag{3c}$$

$$b = -\frac{\sqrt{3}\mathrm{i}\hbar^2}{m_0}\gamma_3(k_x - \mathrm{i}k_y)k_z \tag{3d}$$

$$c = \frac{\sqrt{3}\hbar^2}{2m_0}[\gamma_2(k_x^2 - k_y^2) - 2\mathrm{i}\gamma_3 k_x k_y] \tag{3e}$$

$$q = (H_{v1} - H_{v2})/\sqrt{2}. \tag{3f}$$

Δ_0 is the energy split between the two uppermost valence bands and the spin–orbit band. This spin–orbit split-off energy was obtained from the full-potential band structure calculation and can be parametrized by

$$\Delta_0 = (0.047 + 0.251x)\,\mathrm{eV}; \qquad x \leqslant 0.3. \tag{4}$$

To solve this eigenvalue problem, the Kohn–Luttinger parameters γ_1, γ_2 and γ_3 have to be found. This is carried out by fitting the results from the full-potential band-structure calculation to the eigenvalues of the Kohn–Luttinger Hamiltonian (with varying γ-values). Therefore, a calculation routine, which minimizes the difference in energy between the full self-consistently calculated FPLAPW band energies and the eigenvalues of the Kohn–Luttinger Hamiltonian, is used. About 750 $\boldsymbol{k}$-values with $|\boldsymbol{k}| \leqslant 0.01(2\pi/a)$ in various directions were used.

The Kohn–Luttinger parameters can be described with good accuracy by quadratic functions in composition x:

$$\gamma_1 = 4.5304 + 2.6877x + 2.9908x^2 \tag{5a}$$

$$\gamma_2 = 0.3605 + 0.8461x + 1.9291x^2 \tag{5b}$$

$$\gamma_3 = 1.5163 + 1.1834x + 1.6295x^2. \tag{5c}$$

If the interaction between the two uppermost valence bands and the spin–orbit band is considered to be negligible, the Kohn–Luttinger Hamiltonian can be separated into a 4×4 matrix and a 2×2 matrix. The problem can then be solved analytically [7]. In the present calculation, however, we have used the full 6×6 matrix and instead solved the eigenvalue problem numerically.

Furthermore, the numerical solution has the advantage to give better eigenvectors A_j of the Hamiltonian. The vector components of A_j are the coefficients of a decomposition of the periodic part of the Bloch functions $u^0_{j\sigma}(\boldsymbol{k}', \boldsymbol{r})$ into the pure angular momentum states $\Phi_{j\sigma}(\boldsymbol{k}_0, \boldsymbol{r}) = |3/2, \pm 3/2\rangle, |3/2, \pm 1/2\rangle, |1/2, \pm 1/2\rangle$ for $\boldsymbol{k}_0 = \boldsymbol{0}$

$$u^0_{j\sigma}(\boldsymbol{k}', \boldsymbol{r}) = \sum_{i,\mu} A_{j\sigma,i\mu}(\boldsymbol{k}', \boldsymbol{k_0})\Phi_{i\mu}(\boldsymbol{k}_0, \boldsymbol{r}), \tag{6}$$

where the $A_{j\sigma,i\mu}(\boldsymbol{k}', \boldsymbol{k_0})$ are the matrix elements of the 6×6 eigenstate matrix of the Kohn–Luttinger Hamiltonian. Since $\Phi_{i\mu}(\boldsymbol{k}_0, \boldsymbol{r})$ are orthogonal, the spin independent overlap integrals $\Lambda_{j,j'}(\boldsymbol{k}_0, \boldsymbol{k}')$, which are used in the description of scattering events [24, 25], can easily be calculated for the valence bands:

$$\Lambda_{j,j'}(\boldsymbol{k}_0, \boldsymbol{k}') = \tfrac{1}{2} \sum_{\sigma,\sigma'=\uparrow\downarrow} \left| \int \mathrm{d}\boldsymbol{r}\, u^0_{j\sigma}(\boldsymbol{k}_0, \boldsymbol{r}) u^0_{j'\sigma'}(\boldsymbol{k}', \boldsymbol{r}) \right|^2. \tag{7}$$

To use these energies in a spin independent Green function formalism, we average over $E^0_{j\uparrow}(\boldsymbol{k})$ and $E^0_{j\downarrow}(\boldsymbol{k})$. For Si the spin up band and the spin down band are degenerate. For $Si_{1-x}Ge_x$ ($x > 0$) the difference between $E^0_{j\uparrow}(\boldsymbol{k})$ and $E^0_{j\downarrow}(\boldsymbol{k})$ is small. This averaging therefore only produces a small error.

The approximated energy bands have a better accuracy closer to the Γ-point than far out in the Brillouin zone, because $\boldsymbol{k}$-points in the vicinity of the Γ-point have been weighted stronger in the minimization routine. Nevertheless, we obtain a good agreement between the approximated valence bands and the FPLAPW valence bands down to the Fermi energy of the p-type doped crystal, and we can therefore obtain a good dielectric function (see section 2.2) by using the energy bands and the overlap integrals from the Kohn–Luttinger parametrization.

2.2. Self-energy due to doping

The self-energies are expressed in terms of the unperturbed, time-ordered Green function $G^0_j(\boldsymbol{k}, \omega)$ (for both n- and p-type) and the dielectric function $\tilde{\epsilon}(\boldsymbol{q}, \omega)$ of the electron gas (for n-type $Si_{1-x}Ge_x$) or hole gas (for p-type $Si_{1-x}Ge_x$), respectively.

$$G^0_j(\boldsymbol{k}, \omega) = \frac{\eta^0_j(\boldsymbol{k})}{\omega - \xi^0_j(\boldsymbol{k}) - \mathrm{i}\delta} + \frac{1 - \eta^0_j(\boldsymbol{k})}{\omega - \xi^0_j(\boldsymbol{k}) + \mathrm{i}\delta}; \qquad \xi^0_j(\boldsymbol{k}) = E^0_j(\boldsymbol{k})/\hbar. \tag{8}$$

$\eta_j^0(\boldsymbol{k})$ is the occupation number (i.e., $\eta_j^0(\boldsymbol{k}) = 1$ if $|\boldsymbol{k}, j\rangle$ is occupied and 0 otherwise). δ is a positive infinitesimal small number. Within the RPA and including the local-field correction $\bar{f}(\boldsymbol{q})$ of Hubbard [12], the dielectric function $\tilde{\epsilon}(\boldsymbol{q}, \omega)$ can be written as [10, 14, 26, 27]

$$\tilde{\epsilon}(\boldsymbol{q}, \omega) = 1 - (1 - \bar{f}(\boldsymbol{q}))\frac{2}{\hbar}\frac{v(\boldsymbol{q})}{\kappa}\int \frac{\mathrm{d}\boldsymbol{k}}{(2\pi)^3}\int_{-\infty}^{\infty}\frac{\mathrm{d}\omega'}{2\pi\mathrm{i}}\sum_j G_j^0(\boldsymbol{k}, \omega')G_j^0(\boldsymbol{k}+\boldsymbol{q}, \omega'+\omega). \tag{9}$$

The summation indices are $j = c1$ for n-type materials and $j = v1, v2, v3$ for p-type materials and $v(\boldsymbol{q})$ is the Coulomb potential and κ the static dielectric function of the host material [10, 14, 27]. The local field correction of Hubbard can be written for n-type materials as

$$\bar{f}(\boldsymbol{q}) = \frac{1}{2\nu^2}\sum_{i=1}^{\nu}\frac{E_{c1}^0(\Delta\boldsymbol{k}_i + \boldsymbol{q})}{E_{c1}^0(\Delta\boldsymbol{k}_i + \boldsymbol{q}) + E_F^c}, \tag{10}$$

where $\Delta\boldsymbol{k}_i = \boldsymbol{k}_{0,i} - \boldsymbol{k}_{0,1}$ is the vector between the different equivalent minima of the conduction band and one specific conduction band minimum $\boldsymbol{k}_{0,1}$. ν is the number of conduction band minima ($\nu = 6$ in the case of $Si_{1-x}Ge_x$, $x \leqslant 0.3$), and E_F^c is the Fermi energy of the electron gas in the conduction band. The corresponding expression for p-type materials is

$$\bar{f}(\boldsymbol{q}) = \frac{1}{2\nu_p^2}\sum_{j=v_1}^{v_3}\frac{E_j^0(\boldsymbol{q})\Theta(E_j^0(\boldsymbol{0}) - E_F^v)}{E_j^0(\boldsymbol{q}) + E_F^v}, \tag{11}$$

where ν_p is the number of populated valence bands, $\Theta(E_j^0(\boldsymbol{0}) - E_F^v)$ is the Heaviside step function and E_F^v is the Fermi energy of the hole gas in the valence bands.

For n-type material the energy shifts of the lowest conduction band ΔE_{c1} and of the uppermost valence band ΔE_{v1} are [10, 11]

$$\begin{aligned}\Delta E_j = -\mathrm{Re}\int \frac{\mathrm{d}\boldsymbol{q}}{(2\pi)^3}\int\frac{\mathrm{d}\omega}{2\pi\mathrm{i}}\sum_{j'}\Lambda_{j,j'}(\boldsymbol{k}_0, \boldsymbol{k}')\frac{v(\boldsymbol{q})}{\kappa}\Bigg\{\frac{G_{j'}^0(\boldsymbol{k}', \omega + \xi_j^0(\boldsymbol{k}_0))}{\tilde{\epsilon}(\boldsymbol{q}, \omega)} \\ + \frac{1}{2}\left(\frac{1}{\omega + (\xi_{j'}^0(\boldsymbol{k}') - \xi_j^0(\boldsymbol{k}_0)) - \mathrm{i}\delta} - \frac{1}{\omega - (\xi_{j'}^0(\boldsymbol{k}') - \xi_j^0(\boldsymbol{k}_0)) + \mathrm{i}\delta}\right)\Bigg\} \\ + \mathrm{Re}\int\frac{\mathrm{d}\boldsymbol{q}}{(2\pi)^3}\frac{N_D}{\hbar}\left(\frac{v(\boldsymbol{q})}{\kappa\tilde{\epsilon}(\boldsymbol{q}, 0)}\right)^2\sum_{j'}\Lambda_{j,j'}(\boldsymbol{k}_0, \boldsymbol{k}')G_{j'}^0(\boldsymbol{k}', \xi_j^0(\boldsymbol{k}_0)),\end{aligned} \tag{12}$$

where $\boldsymbol{k}' = \boldsymbol{k}_0 + \boldsymbol{q}$. For the highest valence band maximum $j = v1$ and $\boldsymbol{k}_0 = \boldsymbol{0}$, whereas for one of the six lowest and equivalent conduction band minima $j = c1$ and $\boldsymbol{k}_0 = \boldsymbol{k}_{0,1}$. The different contributions to the energy shift are the exchange–correlation energy (first term in equation (12)), the electrostatic self-interaction (second term) and the electron–donor interaction (third term). N_D is the donor ion concentration.

In figure 2 the different contributions to the energy shift of the lowest conduction band ΔE_{c1} are plotted for n-type (a) and p-type (b) Si. The electron–electron contribution (the exchange–correlation energy plus the electrostatic self-interaction) is about 25% larger than the electron–ion contribution. In the calculation of the dielectric function in equation (9) we include the local-field correction $\bar{f}(\boldsymbol{q})$ of Hubbard [12]. This correction is rather small as can be seen in figure 2, where the dashed lines represent the calculations excluding the Hubbard correction.

Equation (12) is valid for n-type $Si_{1-x}Ge_x$, but one can also use the same expression for p-type material by treating the holes as particles and the electrons as antiparticles. That implies ΔE_j has to be changed to $-\Delta E_j$ and $\xi_j^0(\boldsymbol{k}_0)$ to $-\xi_j^0(\boldsymbol{k}_0)$. Moreover, the donor concentration N_D has to be replaced by the acceptor concentration N_A.

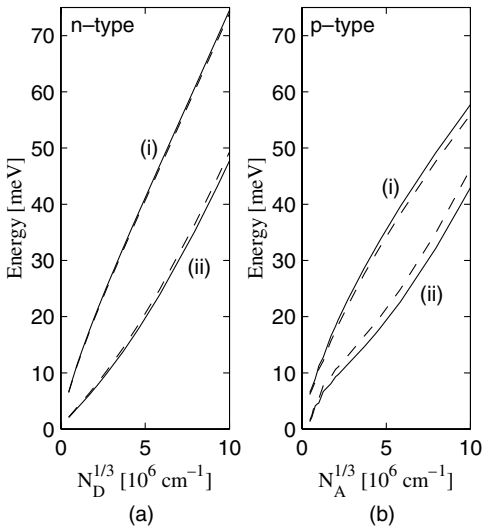

Figure 2. The sum of the exchange–correlation self-energy and the electrostatic self-interaction (i) and the electron–ion contribution (ii) to the shift of the lowest conduction band ΔE_{c1} in n-type (a) and p-type (b) Si. The solid lines represent the calculation including the Hubbard local-field correction. The dashed lines refer to the calculation without the correction.

Equation (9) was calculated analytically assuming parabolic conduction bands (for n-type materials) and spherical valence bands (for p-type materials) for the energies in the two Green functions. For the n-type crystal this holds since we in general assume parabolic conduction bands. For p-type this is a rather bad approximation since the valence bands are very non-parabolic. Instead of taking the effective masses at the valence band maximum to describe the curvature of the energy dispersion relations, we introduce hole concentration dependent density-of-states masses. The masses are chosen in such a way that the band filling corresponds exactly to the Fermi energy E_F^v of the hole gas in the true FPLAPW valence bands. For low concentration only the $v1$- and $v2$-bands are filled with holes and beyond a certain concentration the $v3$-band is also filled. By this treatment the non-parabolicity of the valence bands is considered in an approximate but reasonable way [10]. The concentration dependent density-of-states masses of the three uppermost valence bands are shown in figure 3.

The polarity of the Si–Ge bond can with reasonable accuracy be neglected [28], which means that the zero-frequency transverse optical and longitudinal optical modes are degenerate. We therefore assume that $Si_{1-x}Ge_x$ is nonpolar. From the FPLAPW calculation we obtained the lattice dielectric function in the Si rich regime as

$$\kappa(x) = 12.49 - 0.84x; \qquad x \leqslant 0.3, \tag{13}$$

which for $x = 0$ is slightly larger than the experimental value of Si: $\kappa = 11.7$–12.1 [23].

The overlap integrals $\Lambda_{j,j'}(\boldsymbol{k}_0, \boldsymbol{k}')$ in equation (12) have to be calculated only for the valence bands. For the conduction bands $\Lambda_{c1,c1}(\boldsymbol{k}_0, \boldsymbol{k}')$ can be regarded to be unity, if $\boldsymbol{k}_0$ and $\boldsymbol{k}'$ are in the same minimum [16], and scattering between the six different but equivalent conduction band minima can be neglected [29]. Scattering between the valence bands and the conduction bands is assumed to be negligible since the bandgap of $Si_{1-x}Ge_x$ is relatively large.

Because the two uppermost valence bands are degenerate at the Γ-point, the overlap integrals $\Lambda_{vi,vi'}(\boldsymbol{0}, \boldsymbol{q})$ for $i = 1, 2$ have to be replaced by the average overlap integral $[\Lambda_{v1,vi'}(\boldsymbol{0}, \boldsymbol{q}) + \Lambda_{v2,vi'}(\boldsymbol{0}, \boldsymbol{q})]/2$. In previous calculations [14] the overlap integrals between

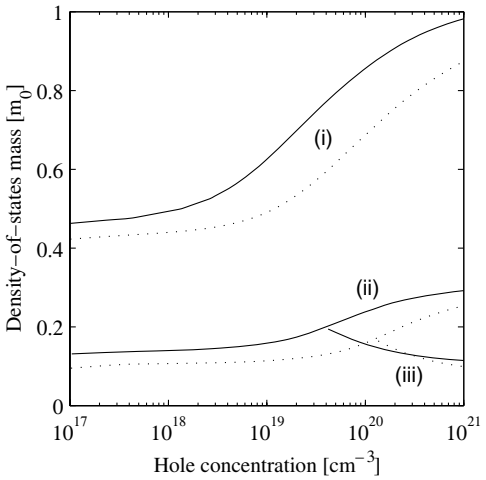

Figure 3. The dielectric function $\tilde{\epsilon}(\boldsymbol{q}, \omega)$ in equation (9) was calculated by introducing the concentration dependent density-of-states masses $m_{v1}(p)$ (i), $m_{v2}(p)$ (ii) and $m_{v3}(p)$ (iii) for the three uppermost valence bands. We show the density-of-states masses of Si (solid curves) and of $Si_{0.7}Ge_{0.3}$ (dotted curves).

different states in the valence bands were approximated by assuming parabolicity of the valence bands and not taking into account the spin–orbit band. The overlap integrals $\Lambda_{vi,vi'}(\boldsymbol{k}, \boldsymbol{k}')$ were approximated by $\Lambda^{app}_{v1,v1}(\Theta) = 0.25 + 0.75\cos^2(\Theta)$, $\Lambda^{app}_{v1,v2}(\Theta) = 0.75\sin^2(\Theta)$ and $\Lambda^{app}_{v1,v3}(\Theta) = 0$ [24]. Θ is the angle between the vectors $\boldsymbol{k}$ and $\boldsymbol{k}'$.

The differences between approximated overlap integrals and those overlap integrals calculated with the $\boldsymbol{k}\cdot\boldsymbol{p}$-method are large, as shown in figure 4. In figure 5, the overlap integrals $\Lambda_{v1,vi}(\boldsymbol{0}, \boldsymbol{k}')$ are plotted in two different directions in the $\boldsymbol{k}$-space. Again, the values are most accurate close to the Γ-point.

3. Results

The outcome of the BGN calculation is presented in figures 6–8. In figure 6, the energy shifts of the lowest conduction band minimum ΔE_{c1} and of the highest valence band maximum ΔE_{v1} are shown as functions of dopant concentration for n-type as well as p-type Si and $Si_{0.7}Ge_{0.3}$. The solid curves represent the present $\boldsymbol{k}\cdot\boldsymbol{p}$-method values. These energy shifts can be parametrized with respect to the dopant concentration. For n-type doping the shifts can be expressed as

$$\Delta E_{c1} = A_{n,c1}(N_D 10^{-18}\ \mathrm{cm}^3)^{1/3} + B_{n,c1}(N_D 10^{-18}\ \mathrm{cm}^3)^{1/2} \tag{14a}$$

$$\Delta E_{v1} = A_{n,v1}(N_D 10^{-18}\ \mathrm{cm}^3)^{1/4} + B_{n,v1}(N_D 10^{-18}\ \mathrm{cm}^3)^{1/2}. \tag{14b}$$

The parametrization was originally presented by Jain and Roulston [13] expounded from a semi-empirical description and by using the parabolic approximation. Here, we also use the expansion for the more complete Green function model and in the full band-structure calculations. For p-type doping the corresponding expressions are

$$\Delta E_{c1} = A_{p,c1}(N_A 10^{-18}\ \mathrm{cm}^3)^{1/4} + B_{p,c1}(N_A 10^{-18}\ \mathrm{cm}^3)^{1/2} \tag{15a}$$

$$\Delta E_{v1} = A_{p,v1}(N_A 10^{-18}\ \mathrm{cm}^3)^{1/3} + B_{p,v1}(N_A 10^{-18}\ \mathrm{cm}^3)^{1/2}. \tag{15b}$$

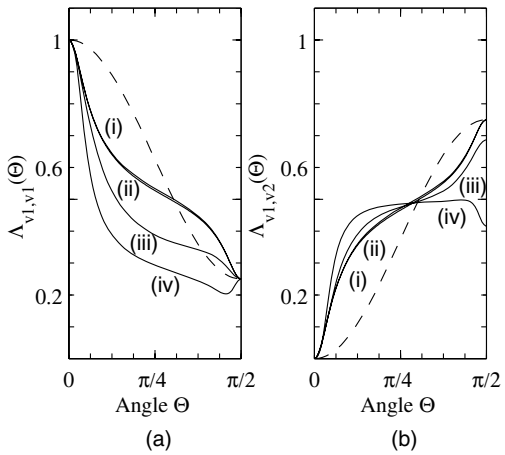

Figure 4. Overlap integrals $\Lambda_{v1,j}$ in Si between initial state $\boldsymbol{k}$ in the uppermost valence band and final states $\boldsymbol{k}'$ in the uppermost valence band $j = v1$ (a) and the second uppermost valence band $j = v2$ (b) as functions of angle Θ between $\boldsymbol{k}$ and $\boldsymbol{k}'$. The lengths of the wavevectors are $k = 0.001$ and $k' = 0.001$ (i), $k' = 0.01$ (ii), $k' = 0.05$ (iii) and $k' = 0.1$ (iv) in units of $(2\pi/a)$. The results for different compositions of Si and Ge are similar. The dashed curves are the commonly used approximations $\Lambda^{app}_{v1,v1}$ (a) and $\Lambda^{app}_{v1,v2}$ (b).

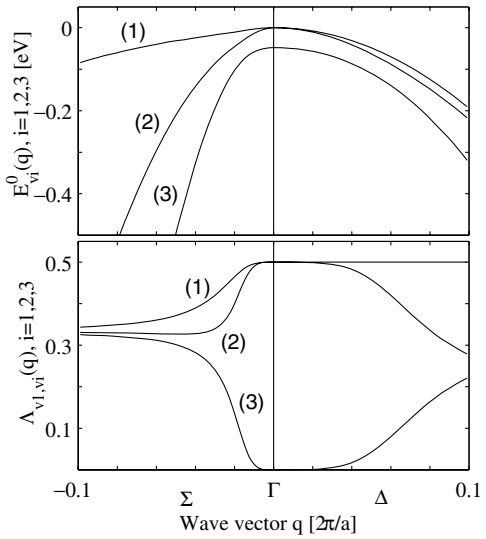

Figure 5. Energies and overlap integrals of the three uppermost valence bands $v1$ (1), $v2$ (2) and $v3$ (3) of Si in the directions $\Gamma X = \Delta$ (right-hand side of the figure) and $\Gamma K = \Sigma$ (left-hand side).

N_D and N_A are the donor and acceptor concentrations, respectively, in units of cm^{-3}. The fitted parameters in terms of composition $x \leqslant 0.3$ are shown in table 1. The maximum error of the parametrization is 4 meV. For different compositions of $Si_{1-x}Ge_x$ ($x \leqslant 0.3$) the results are almost the same. This is not surprising, since the band structure of the intrinsic crystal does not change much, as can be seen from the small changes of the γ-values with varying x (see equation (5)). Because of these small differences, we have only presented the results for $x = 0$

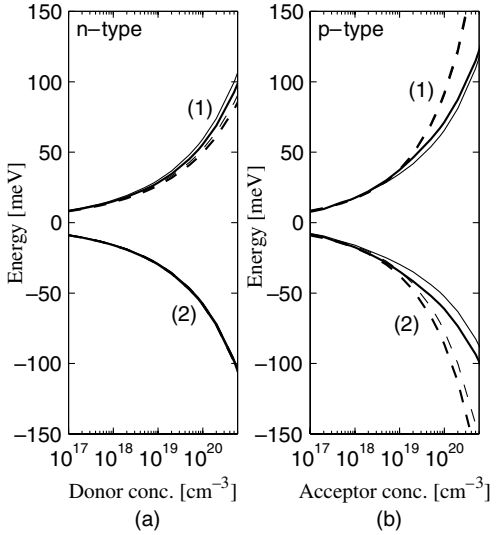

Figure 6. Energy shifts of the uppermost valence band maximum ΔE_{v1} (1) and the lowest conduction band minimum ΔE_{c1} (2) in n-type (a) and p-type (b) Si (thin curves) and $Si_{0.7}Ge_{0.3}$ (thick curves), obtained with the 6×6 Hamiltonian matrix. The dashed curves refer to the parabolic approximation.

Table 1. Parameters describing the energy shifts of the conduction band minimum and of the valence band maximum as functions of composition x, see equations (14) and (15).

n-type:	$A_{n,c1}(x) = -13.9554 - 2.6464x - 3.7560x^2$ meV
	$B_{n,c1}(x) = 0.5781 + 0.2951x - 0.1021x^2$ meV
	$A_{n,v1}(x) = 14.3045 - 1.1039x - 3.0072x^2$ meV
	$B_{n,v1}(x) = 1.4416 - 0.5516x - 0.3467x^2$ meV
p-type:	$A_{p,c1}(x) = -15.2906 - 12.8051x + 9.4402x^2$ meV
	$B_{p,c1}(x) = -0.4845 + 0.9021x - 1.4899x^2$ meV
	$A_{p,v1}(x) = 16.5817 + 12.1164x - 16.3495x^2$ meV
	$B_{p,v1}(x) = -0.9045 - 3.0309x + 4.2782x^2$ meV

and 0.3 in the figures. Nevertheless, the parametrization of $A_{n,c1}$, $B_{n,c1}$ etc was determined with the values for $x = 0$, 0.1, 0.2 and 0.3.

The dashed curves in figures 5 and 6 refer to the parabolic approximation of the valence bands. Here we used the effective masses at the Γ-point of the $\boldsymbol{k} \cdot \boldsymbol{p}$-perturbation method, averaged over all directions in $\boldsymbol{k}$-space. The masses can be parametrized in terms of composition x for $x \leqslant 0.3$ by

$$m_{v1}(x) = (0.4626 - 0.1584x + 0.1248x^2)\, m_0 \tag{16a}$$

$$m_{v2}(x) = (0.1410 - 0.1103x + 0.0048x^2)\, m_0 \tag{16b}$$

$$m_{v3}(x) = (0.2006 - 0.1031x - 0.0576x^2)\, m_0. \tag{16c}$$

For Si these spherical effective mass values are in good agreement with experimental values: $m_{v1} = 0.537\, m_0$, $m_{v2} = 0.153\, m_0$ and $m_{v3} = 0.234\, m_0 - 0.29\, m_0$ [23].

In figure 7, the reduced bandgap $E_g^2 = E_g^0 + \Delta E_{c1} - \Delta E_{v1}$ and the optical bandgap E_g^1 are plotted versus the dopant concentration for Si and $Si_{0.7}Ge_{0.3}$. We have used the experimental value of the fundamental bandgap of the undoped crystal: $E_g^0(x) = (1.155 -$

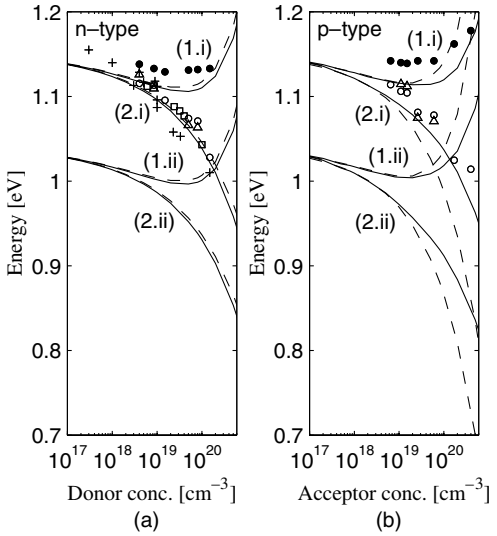

Figure 7. Optical E_g^1 (1) and reduced E_g^2 (2) bandgap energies in n-type (a) and p-type (b) Si (i) and $Si_{0.7}Ge_{0.3}$ (ii). The solid curves represent the calculation with the 6×6 Hamiltonian matrix. The dashed curves refer to the parabolic approximation. Also shown are the experimental values of the reduced bandgap in n-type Si by Wagner and del Alamo [31] (open circles and triangles), by Dumke [32] (squares) and by Lanyon and Tuft [33] (plus signs). For p-type Si we show experimental values of the reduced bandgap by Wagner and del Alamo [31] (open circles and triangles). Filled circles refer to the measured optical bandgap by Wagner and del Alamo [31], for both n-type and p-type Si.

$0.43x + 0.206x^2$) eV for $x \leqslant 0.85$ [30]. The optical bandgap was calculated by neglecting changes of the band curvature, i.e., the Fermi energy E_F of the doped crystal was obtained by assuming the band structure of the intrinsic one: $E_g^1 = E_g^2 + E_F$. This approximation causes negligible errors [10], especially in non-polar materials where band tailoring due to polaron interaction is absent.

In the figure, we have indicated some collective experimental values of the reduced bandgap in n-type Si (plus signs), presented by Lanyon and Tuft [33]. The squares show the corresponding results of photoluminescence (PL) measurements performed by Dumke [32]. Here, the reduced bandgap was determined by fitting the luminescence peaks to a semi-empirical expression including broadening due to finite resolution of emission spectra, incomplete thermalization of carriers and lifetime effects.

Open circles and triangles represent the PL measurements of the reduced bandgap in n-type Si:P and p-type Si:B by Wagner and del Alamo [31], determined from a line shape analysis of the low-energy edge of the PL spectra. The filled circles are the corresponding measured data of the optical bandgap, given by the high-energy cut-off of the PL spectra [31]. Overall, our calculations are in good agreement with these experimental data, although the optical bandgap is slightly underestimated.

In figure 8, we present the PL data of the BGN in p-type boron doped Si/Si(p^+)/Si(p) pseudoheterostructures and Si/$Si_{0.82}Ge_{0.18}$(p^+)/Si(p) heterostructures measured by Souifi *et al* [34]. The filled triangles and rectangles indicate the BGN ($\Delta E_{v1} - \Delta E_{c1}$) in Si and $Si_{0.82}Ge_{0.18}$, respectively. For comparison, we include the PL results of bulk Si:B of Wagner and del Alamo [31] (open circles). The result of Souifi *et al* shows only small effects on the BGN due to composition, which is in agreement with our findings (solid lines in the figure).

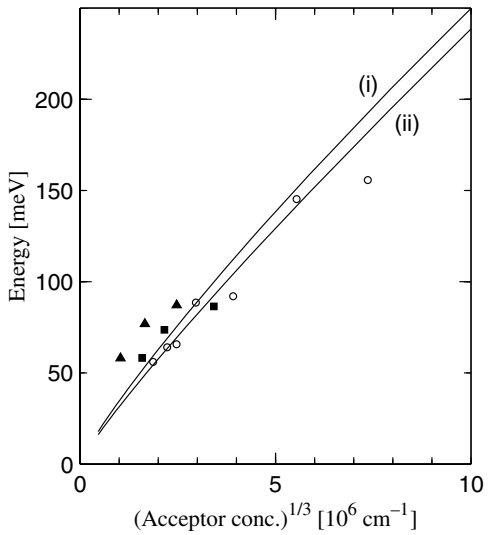

Figure 8. The BGN ($\Delta E_{v1} - \Delta E_{c1}$) in p-type Si (i) and $Si_{0.82}Ge_{0.18}$ (ii) calculated from the parametrization of equation (15). Also shown are the experimental values of the BGN in Si/Si(p$^+$)/Si(p) (filled circles) and Si/$Si_{0.82}Ge_{0.18}$(p$^+$)/Si(p) (filled triangles) by Souifi *et al* [34], and in p-type Si (open circles) by Wagner and del Alamo [31].

For n-type doping the calculations with parabolic and non-parabolic valence bands (this also implies approximated and correct overlap integrals, respectively) lead to similar results. That is reasonable, although the approximated overlap integrals $\Lambda^{app}_{vi,vi'}(\boldsymbol{k}, \boldsymbol{k}')$ look quite different from the calculated ones on the first view (figure 4). However, the average over all angles Θ is alike.

For p-type doping and for large concentrations the BGN obtained by using the parabolic energy bands and the BGN obtained by using the Kohn–Luttinger Hamiltonian differ strongly. This can been seen in figure 6(b) where the two curves describing the BGN deviate strongly for $N_A > 10^{19}$ cm^{-3}. A hole concentration of 10^{19} cm^{-3} corresponds to a Fermi energy of about $\Delta_0/2$, and above this concentration the influence of the $v3$-band becomes recognizable since the interaction of the $v1$- and $v2$-bands with the $v3$-band leads to a deformation of the three uppermost valence bands (see figure 5). This deformation affects the band filling, and therefore also the Fermi energy. It has been shown [10] that a good determination of the Fermi energy is crucial in order to accurately calculate the BGN. As expected the calculation of E_g^2 using the Kohn–Luttinger Hamiltonian gives a better agreement with the experimental data than the calculation with parabolic bands. Furthermore, using the parabolic approximation would lead to a much more underestimated optical bandgap in p-type materials than the present $\boldsymbol{k} \cdot \boldsymbol{p}$-method.

4. Summary

The BGN in Si and $Si_{1-x}Ge_x$ ($x \leqslant 0.3$) due to n-type and p-type doping has been calculated with a Green function formalism. The band structure of the intrinsic crystal and the overlap integrals were approximated within the $\boldsymbol{k}\cdot\boldsymbol{p}$-method. The valence bands are in good agreement with the band structure obtained from the FPLAPW calculation in the region of the Brillouin zone of interest in the present investigation. The calculated values of the BGN were found

to be in very good agreement with the experimental data. It has also turned out that the non-parabolicity of the valence bands leads to a significant reduction of the BGN at high dopant concentration compared to the calculation with parabolic valence bands. Therefore it is necessary to use a non-parabolic description of these bands. The calculated values of the BGN for Si and for $Si_{0.7}Ge_{0.3}$ differ only slightly.

There are a few effects that have not been taken into account but are of great interest. The strain of the material in certain directions lowers the symmetry of the crystal and therefore leads to band splitting, which is important especially at the valence band maximum. This will affect, for instance, the band filling in p-type materials. Moreover, we have only calculated the crystal properties at zero absolute temperature. Temperature has the effect of lifting electrons from the valence up to the conduction band, which then will contribute to the screening. For moderate temperatures, however, the temperature-dependent band filling in Si rich $Si_{1-x}Ge_x$ is much lower than the critical concentration of the Mott transition. Nevertheless, the excitations will affect the self-energy through the poles of the dielectric function [35].

Acknowledgment

This work was financially supported by the Swedish Research Council (VR).

References

[1] Jain S C, Decoutere S, Willander M and Maes H E 2001 *Semicond. Sci. Technol.* **16** R51
[2] Jain S C, Decoutere S, Willander M and Maes H E 2001 *Semicond. Sci. Technol.* **16** R67
[3] Keyes R W 1977 *Comments Solid State Phys.* **7** 149
[4] Luttinger J M and Kohn W 1955 *Phys. Rev.* **97** 869
[5] Singh J 1993 *Physics of Semiconductors and their Heterostructures* (New York: McGraw-Hill)
[6] Kane E O 1956 *J. Phys. Chem. Solids* **1** 82
[7] Dresselhaus G, Kip A F and Kittel C 1955 *Phys. Rev.* **98** 368
[8] Mott N F and Davis E A 1979 *Electronic Processes in Non-Crystalline Materials* 2nd edn (Oxford: Clarendon)
[9] Blaha P, Schwarz K and Luitz J 1999 *WIEN97, a Full Potential Linearized Augmented Plane Wave Package for Calculating Crystal Properties* Technical University of Vienna (ISBN 3-9501031-0-4)
This is an improved and updated Unix version of the original copyrighted WIEN code, which was published by Blaha P, Schwarz K, Sorantin P and Trickey S B 1999 *Comput. Phys. Commun.* **59** 399
[10] Persson C, Lindefelt U and Sernelius B E 1999 *Phys. Rev.* B **60** 16479
[11] Sernelius B E and Berggren K-F 1981 *Phil. Mag.* B **43** 115
[12] Hubbard J 1957 *Proc. R. Soc.* A **243** 336
[13] Jain S and Roulston D J 1991 *Solid-State Electron.* **34** 453
[14] Sernelius B E 1986 *Phys. Rev.* B **34** 5610
[15] Persson C, Ahuja R and Johansson B 2001 *Phys. Rev.* B **64** 033201
[16] Persson C, Lindefelt U and Sernelius B E 1999 *J. Appl. Phys.* **86** 4419
[17] Perdew J P and Wang Y 1992 *Phys. Rev.* B **45** 13244
[18] Ceperley D M and Alder B J 1980 *Phys. Rev. Lett.* **45** 566
[19] Logan R A, Rowell J M and Trumbore F A 1964 *Phys. Rev.* **136** A1751
[20] Persson C and Lindefelt U 1996 *Phys. Rev.* B **54** 10257
[21] Faulkner J S 1982 *Prog. Mater. Sci.* **27** 3
[22] Krishnamurthy S, Sher A and Chen A-B 1986 *Phys. Rev.* B **33** 1026
[23] Madelung O *et al* (ed) 1982 *Numerical Data and Functional Relationships in Science and Technology (Springer New Series vol III/17a)* (Berlin: Springer)
[24] Combescot M and Noziéres P 1972 *Solid State Commun.* **10** 301
[25] Berggren K-F and Sernelius B E 1981 *Phys. Rev.* B **24** 1971
[26] Sernelius B E 1987 *Phys. Rev.* B **36** 4878
[27] Mahan G D 1990 *Many-Particle Physics* 2nd edn (New York: Plenum)
[28] Schmid U, Cardona M and Christensen N E 1990 *Phys. Rev.* B **41** 5919
[29] Berggren K-F and Sernelius B E 1984 *Phys. Rev.* B **29** 5575

[30] Weber J and Alonso M I 1989 *Phys. Rev.* B **40** 5683
[31] Wagner J and del Alamo J A 1988 *J. Appl. Phys.* **63** 425
[32] Dumke W P 1983 *Appl. Phys. Lett.* **42** 196
[33] Lanyon H P D and Tuft R A 1979 *IEEE Trans. Electron Devices* **26** 1014
[34] Souifi A, Brémond G, Benyattou T, Guillot G, Dutartre D and Warren P 1993 *Appl. Phys. Lett.* **62** 2986
[35] Thuselt F and Rösler M 1985 *Phys. Status Solidi* b **130** 661